Overcoming the Time Limitation in Molecular Dynamics Simulation of Crystal Nucleation: A Persistent-Embryo Approach

Yang Sun,[1,*] Huajing Song,[1] Feng Zhang,[1,†] Lin Yang,[1] Zhuo Ye,[1] Mikhail I. Mendelev,[1] Cai-Zhuang Wang,[1,2] and Kai-Ming Ho[1,2,3]

[1]*Ames Laboratory, U.S. Department of Energy, Ames, Iowa 50011, USA*
[2]*Department of Physics, Iowa State University, Ames, Iowa 50011, USA*
[3]*Hefei National Laboratory for Physical Sciences at the Microscale and Department of Physics, University of Science and Technology of China, Hefei, Anhui 230026, China*

(Received 23 August 2017; revised manuscript received 4 December 2017; published 23 February 2018)

The crystal nucleation from liquid in most cases is too rare to be accessed within the limited time scales of the conventional molecular dynamics (MD) simulation. Here, we developed a "persistent embryo" method to facilitate crystal nucleation in MD simulations by preventing small crystal embryos from melting using external spring forces. We applied this method to the pure Ni case for a moderate undercooling where no nucleation can be observed in the conventional MD simulation, and obtained nucleation rate in good agreement with the experimental data. Moreover, the method is applied to simulate an even more sluggish event: the nucleation of the $B2$ phase in a strong glass-forming Cu-Zr alloy. The nucleation rate was found to be 8 orders of magnitude smaller than Ni at the same undercooling, which well explains the good glass formability of the alloy. Thus, our work opens a new avenue to study solidification under realistic experimental conditions via atomistic computer simulation.

DOI: 10.1103/PhysRevLett.120.085703

Homogeneous crystal nucleation from an undercooled liquid is a fundamental process that plays an important role in numerous areas ranging from materials science to biophysics [1]. In classical nucleation theory (CNT), the nucleation is described as a competition between the energy gain associated with the transformation of the bulk liquid into a crystal phase and the energy cost of creating a solid-liquid interface such that the change in the free energy associated with the formation of a nucleus containing N atoms can be presented as

$$\Delta G(N) = N\Delta\mu + s(N/\rho)^{2/3}\gamma, \tag{1}$$

where ρ is the atomic density, $\Delta\mu(<0)$ is the chemical potential difference between the bulk solid and liquid, $\gamma(>0)$ is the solid-liquid interfacial free energy, and s is a factor to account for the nucleus shape. As schematically shown in Fig. 1(a), this competition between the bulk and interface terms leads to a critical barrier ΔG^* where the nucleus reaches the critical size N^*. The low probability of overcoming this free energy barrier makes it inefficient to sample nucleation events in conventional MD simulations [2]. To circumvent this difficulty, advanced sampling techniques such as umbrella sampling [3–5] and metadynamics [6] can be used. With the help of biased potentials, these techniques can, in principle, map out the free energy barrier for nucleation. However, they do not directly give the correct kinetics of the unbiased system, and thus other methods, such as kinetic Monte Carlo (KMC) simulations, have to be used to obtain necessary kinetic parameters for evaluating the nucleation rate [7], which significantly adds to the complexity of the problem. The critical nucleus size was also determined by embedding a large crystal cluster into the liquid and watching if the cluster grows or disappears [8]. Although this method can provide a fast

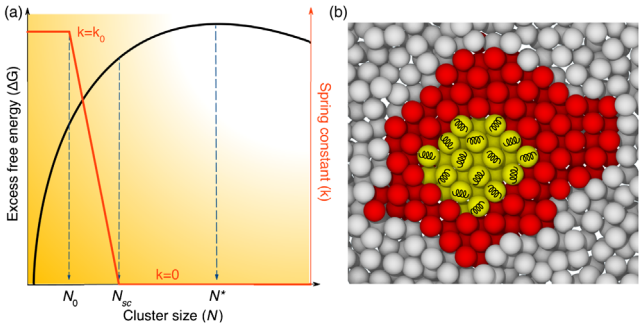

FIG. 1. Using the persistent-embryo method to reach the critical nucleus. (a) The excess free energy (black) and spring constant (red) as a function of the crystalline cluster size N. N_0 is the number of atoms in the constrained embryo. The red curve shows that the strength of the spring constant decreases with the increasing cluster size. The spring is completely removed when the cluster size reaches the threshold value N_{sc}. N^* is the critical size. (b) A cross section of the as-grown crystalline cluster around embryo. The yellow atoms with spring icon are the persistent embryo. The red are the as-grown atoms, showing the crystalline packing. The gray are the liquid atoms.

estimation of the critical nucleus size [9–11], the initial equilibration process during which the cluster should melt, can lead to a considerable overestimation of the critical nucleus size [12]. Moreover, the artificially chosen initial cluster can lead to an unreal description of the nucleus shape, such as the nonspherical nucleus shape in the Lennard-Jones system reviewed recently by Sosso *et al.* in Ref. [2].

In the present study, we took advantage of the well-known fact that the dependence of ΔG on N has a convex shape [see Fig. 1(a)], which means that a large fraction of ΔG^* must be overcome only to grow a small crystalline cluster (embryo). Thus, if the embryo can be kept from remelting, it can reach the critical size even during a relatively short MD simulation. Therefore, we propose a persistent-embryo method to achieve this, in which external spring forces are applied to constrain the embryo from melting. First, we create a crystalline embryo with N_0 atoms (N_0 is much smaller than N^*), which is then inserted into the liquid while a *tunable* harmonic potential is added to each atom in the embryo to effectively keep it from melting. As the embryo grows, the harmonic potential is gradually weakened and is completely removed when the cluster size reaches a subcritical threshold $N_{\mathrm{sc}}(< N^*)$: the spring constant corresponding to the harmonic potential is set as $k(N) = k_0[(N_{\mathrm{sc}} - N)/(N_{\mathrm{sc}})]$ if $N < N_{\mathrm{sc}}$ and $k(N) = 0$ otherwise. If the nucleus melts the harmonic potential is gradually enforced. The strategy to adjust the spring constant to zero before reaching the critical nucleus size ensures the dynamics of the system is unbiased at the critical point, which is an advantage of this approach compared to others such as the lattice mold method [16]. A schematic of the simulation configuration is shown in Fig. 1(b). We emphasize since the springs are removed well before the nucleus reaches the critical size, the overall process simulates homogeneous nucleation.

During the MD simulation, the NPT ensemble is applied with Nose-Hoover thermostats. The time step of the simulation is 1.0 fs. The sample size is set up to 32 000 atoms which is at least 10 times larger than the critical nucleus size. The Finnis-Sinclair (FS) potentials [17] were used for the investigation of Ni [18] and CuZr [19] systems. These FS potentials were developed to accurately reproduce the melting point data and the liquid structure. The initial liquid is equilibrated for 1 ns. The embryo is inserted in the liquid by removing liquid atoms that are closer to the embryo atoms than 2.0 Å. All the simulations were performed using the GPU-accelerated LAMMPS code [20–22]. To quickly identify the solidlike and liquidlike atoms during MD simulation, the widely used bond-orientational order parameter [23,24] is employed by calculating $S_{ij} = \sum_{m=-6}^{6} q_{6m}(i) q_{6m}^*(i)$ between two neighboring atoms based on the Steinhardt parameter $q_{6m}(i) = [1/N_b(i)] \times \sum_{j=1}^{N_b(i)} Y_{lm}(\vec{r}_{ij})$, where $Y_{lm}(\vec{r}_{ij})$ is the spherical harmonics and $N_b(i)$ is the number of nearest neighbors of atom i. Two neighboring atoms i and j are considered to be connected when S_{ij} exceeds a threshold. The threshold is carefully chosen based on Espinosa *et al.*'s "equal mislabeling" method [11], which gives the lowest probability to mislabel the liquid and solid (see Supplemental Material [12] for details). The atoms with 6 connected neighbors are recognized as solidlike. Then the cluster analysis [25], which uses the crystalline bond length as the cutoff distance to choose neighbor atoms, is applied to measure the size of the solid cluster that formed around the initial embryo.

We first applied this method to the pure Ni case with a wide range of moderate undercooling. Under these conditions, experimental nucleation events occur on the time scale of seconds [26] and, hence, cannot be observed in the conventional MD simulation with the simulation time usually less than 1 μs. With the help of a persistent embryo, the long-time fluctuation of the nucleation with nucleus smaller than the embryo is suppressed. The barrier to be overcome by the simulation is reduced so that the nucleation can be observed at the typical MD time scale. When the nucleus reaches the critical size, it has equal chance to dissolve or further grow. Thus, one should expect that the size of the nucleus will fluctuate about N^* within an extended time, which will result in a plateau at the critical region on the $N(t)$ curve. This unique signal can help us to accurately measure N^* in our simulations. We, therefore, launched multiple independent MD runs (up to 50 runs) to collect such critical plateaus for statistical analysis. An example is shown in Fig. 2(a) (see more examples in the Supplemental Material [12]). Although the length of the plateaus varies in different runs, their heights are almost identical. Thus, the critical size can be determined statistically by averaging over all the plateau heights. The obtained critical nucleus size as a function of temperature is shown in Fig. 2(b). We note that as long as the N_0 and N_{sc} are chosen such that the fluctuating plateau can be observed within the typical MD time scale in the simulations, different choices of the embryo shape, N_0 and N_{sc} give a consistent measurement of the critical nucleus size (see Supplemental Material for details [12]). The fundamental reason that the persistent-embryo method allows an accurate measurement of the critical nucleus size is that one can observe the actual fluctuations of a critical nucleus in an unbiased environment and perform extensive statistical analysis based on these fluctuations. This unique feature will be even more important for treating stoichiometric compounds with larger anisotropy of the interfacial properties [28].

In the CNT, the nucleation rate J can be expressed as $J = \kappa \exp(-\Delta G^*/k_B T)$, where k_B is the Boltzmann constant, and κ is a kinetic prefactor. ΔG^* is related to the driving force $|\Delta\mu|$ and the critical size N^* as $\Delta G^* = \frac{1}{2}|\Delta\mu| N^*$ (see Supplemental Material [12]). Using the steady-state model to derive the kinetic prefactor [1], we can express the nucleation rate as

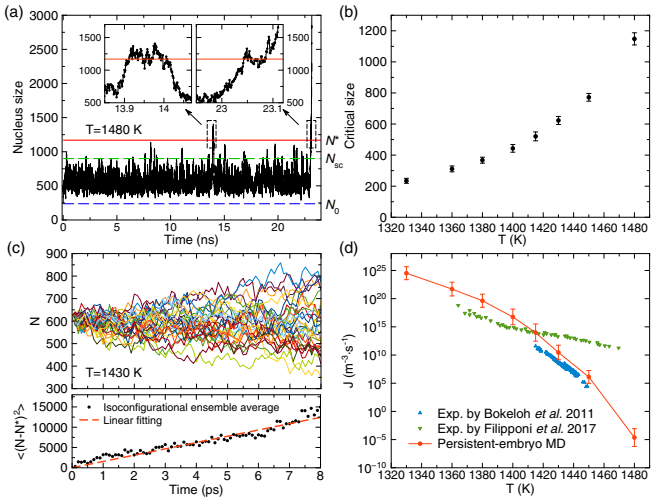

FIG. 2. The persistent-embryo MD simulation of the crystal nucleation in the undercooled liquid Ni. (a) The nucleus size versus time of one Ni nucleation trajectory at 1480 K. The blue dashed line shows the atom number N_0 in the persistent embryo. The green dashed line indicates the threshold to remove the spring and the red solid line indicates the critical size N^*. Two insets enlarge two plateaus at the critical size. (b) The critical size as a function of the temperature. (c) The upper panel shows the nucleus size versus time for the isoconfigurational ensemble with 30 MD runs. Each color indicates an independent MD trajectory. The bottom panel shows the ensemble average of $|\Delta N^*(t)|^2 = |N(t) - N^*|^2$. The dashed line indicates the linear fitting to the first 5 ps to derive the attachment rate. (d) The nucleation rate as a function of the temperature for Ni. The simulation results are connected to guide the eye. The experimental data are from Ref. [26] (upward triangle) and Ref. [27] (downward triangle).

$$J = \rho_L f^+ \sqrt{\frac{|\Delta\mu|}{6\pi k_B T N^*}} \exp\left(-\frac{|\Delta\mu| N^*}{2 k_B T}\right), \qquad (2)$$

where f^+ is the attachment rate of a single atom to the critical nucleus and ρ_L is the liquid density. $\Delta\mu$ can be computed by integrating the Gibbs-Helmholtz equation from the undercooling temperature to the melting point [29]. Following the pioneering work by Auer and Frenkel [7], once the critical nucleus is available, the attachment rate can be measured with MD simulation as the effective diffusion constant for the change in critical nucleus size: $f^+ = \langle|\Delta N^*(t)|^2\rangle/(2t)$. Figure 2(c) shows the measurement of the attachment rate at the critical nucleus using an isoconfigurational ensemble [30]. 30 independent MD runs were performed starting from the same atomic configuration with a critical nucleus but with atomic momenta randomly assigned using the Maxwell distribution. As there are no constraints in the embryos anymore, the critical nucleus indeed melted in half of the MD runs and grew in the other half runs, which further validates the determination of the critical nucleus size.

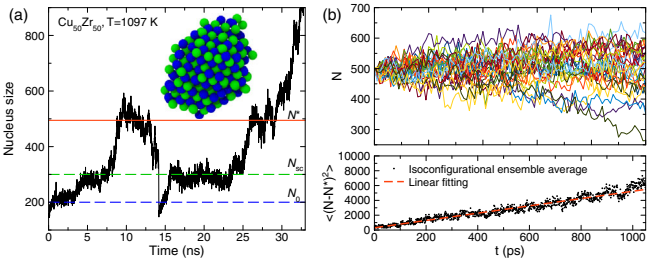

FIG. 3. The persistent-embryo MD for $B2$ nucleation in $Cu_{50}Zr_{50}$ undercooled liquid at 1097 K. (a) Nucleus size as a function of time. The inset shows the $B2$ critical nucleus. (b) 30 MD runs starting from the configuration with critical nucleus are performed. Each color indicates an independent MD trajectory. The dashed line shows the linear fitting of the ensemble average to derive the attachment rate.

Figure 2(d) shows the nucleation rate in pure Ni as a function of temperature. The nucleation rate computed with the persistent-embryo MD covers a wide undercooling range, which can be compared directly to the recent experimental measurements [26,27]. The results agree well with Bokeloh *et al.*'s experimental measurements from 1400 to 1450 K, in which homogeneous nucleation was carefully probed [26]. Our results slightly deviate from Filipponi *et al.*'s measurements [27] from 1360 to 1380 K but these data could be affected by possible heterogeneous nucleation [27].

Compared to the pure Ni case, it is a much more challenging task to simulate a nucleation in a glass-forming alloy, because the crystal nucleation can be bypassed even on the experimental time scale in such a system. Here, we employ the persistent-embryo method to simulate the B2 phase nucleation in the $Cu_{50}Zr_{50}$ alloy, which has attracted extensively attention as a strong binary glass former [31,32]. As shown in Fig. 3(a), we can still obtain the critical nucleus size by sampling plateaus on $N(t)$ curves collected in different MD runs. It is interesting to note that the plateau can sustain much longer time in CuZr than in Ni. This can be attributed to a much slower attachment or detachment rate, which was measured in isoconfigurational simulations shown in Fig. 3(b).

The nucleation rate of the $B2$ phase from the $Cu_{50}Zr_{50}$ liquid alloy was found to be 8 orders of magnitude smaller than the nucleation of the fcc phase in liquid Ni. This explains why the $Cu_{50}Zr_{50}$ liquid can bypass the crystal phase and be driven to the glassy state when cooled at a sufficiently fast rate. In Table I, we compare several factors that could affect the nucleation rates in liquid Ni and $Cu_{50}Zr_{50}$ alloy at the same undercooling $T' = (T_m - T)/T_m$. The examination of this table shows that 6 orders of magnitude are caused by the higher free energy barrier and remaining 2 orders of magnitude result from the smaller attachment rate. The higher nucleation barrier of the $B2$ phase in the $Cu_{50}Zr_{50}$ alloy is associated with much larger energy penalty of forming the liquid-$B2$ interface

TABLE I. The critical nucleus size (N^*), free energy barrier contribution ($e^{-\Delta G^*/k_BT}$), attachment rate (f^+), prefactor (κ), nucleation rate (J), and atomic diffusivity (D) for the pure Ni and $Cu_{50}Zr_{50}$ liquid alloy at same undercooling $T' = [(T_m - T)/(T_m)]$.

System	T (K)	T'	N^*	$e^{-\Delta G^*/k_BT}$	$f^+(s^{-1})$	$\kappa(m^{-3}\,s^{-1})$	$J(m^{-3}\,s^{-1})$	$D(m^2/s)$
Ni	1430	17%	623	1.0×10^{-31}	7.6×10^{14}	2.8×10^{41}	2.9×10^{10}	2.0×10^{-9}
$Cu_{50}Zr_{50}$	1097	17%	495	9.8×10^{-38}	2.5×10^{12}	8.3×10^{38}	81.3	Cu: 9.8×10^{-10} Zr: 7.2×10^{-10}

comparing to that for the liquid-fcc interface in Ni (see Supplemental Material for details [12]). Note the diffusivities of Ni and $Cu_{50}Zr_{50}$ are quite similar. Thus, the attachment rate may be highly affected by the structure of solid-liquid interface as observed by Tang and Harrowell [33].

In summary, the proposed persistent-embryo method dramatically extends the ability of the MD simulation to explore the rare nucleation without the use of biasing forces near the critical point. The spontaneously formed critical nucleus, the critical size, and the kinetic prefactor can be measured so that the nucleation rate can be computed in the CNT framework. The study of the nucleation in pure Ni demonstrated a good agreement with available experimental data proofing the reliability of the preformed work. The investigation of the nucleation in the $Cu_{50}Zr_{50}$ liquid alloy revealed an extremely low nucleation rate that explains the high glass formability of this alloy. These successes demonstrate that our work opens a practical way to quantitatively estimate nucleation rates under realistic experimental conditions.

We thank M. J. Kramer, R. E. Napolitano, X. Song, and R. T. Ott from Ames Laboratory for valuable discussion. Work at Ames Laboratory was supported by the U.S. Department of Energy, Basic Energy Sciences, Materials Science and Engineering Division, under Contract No. DE-AC02-07CH11358, including a grant of computer time at the National Energy Research Scientific Computing Center (NERSC) in Berkeley, CA. K. M. H. acknowledges support from USTC Qian-Ren B (1000-Talents Program B) fund. The Laboratory Directed Research and Development (LDRD) program of Ames Laboratory supported the use of GPU computing.

*yangsun@ameslab.gov
†fzhang@ameslab.gov

[1] K. F. Kelton and A. L. Greer, *Nucleation in Condensed Matter: Application in Materials and Biology* (Elsevier, Amsterdam, 2010).
[2] G. C. Sosso, J. Chen, S. J. Cox, M. Fitzner, P. Pedevilla, A. Zen, and A. Michaelides, Chem. Rev. **116**, 7078 (2016).
[3] G. M. Torrie and J. P. Valleau, J. Comput. Phys. **23**, 187 (1977).
[4] S. Kumar, J. M. Rosenberg, D. Bouzida, R. H. Swendsen, and P. A. Kollman, J. Comput. Chem. **13**, 1011 (1992).
[5] S. Auer and D. Frenkel, Nature (London) **409**, 1020 (2001).
[6] A. Laio and M. Parrinello, Proc. Natl. Acad. Sci. U.S.A. **99**, 12562 (2002).
[7] S. Auer and D. Frenkel, J. Chem. Phys. **120**, 3015 (2004).
[8] X.-M. Bai and M. Li, J. Chem. Phys. **122**, 224510 (2005).
[9] E. Sanz, C. Vega, J. R. Espinosa, R. Caballero-Bernal, J. L. F. Abascal, and C. Valeriani, J. Am. Chem. Soc. **135**, 15008 (2013).
[10] T. Mandal and R. G. Larson, J. Chem. Phys. **146**, 134501 (2017).
[11] J. R. Espinosa, C. Vega, C. Valeriani, and E. Sanz, J. Chem. Phys. **144**, 034501 (2016).
[12] For the Ni potential studied in the present paper, the conventional seeding method systematically overestimates the critical nucleus size which leads to an error of ~3 orders of magnitude on the nucleation rate compared to the persistent-embryo method and the burte-force MD. See Supplemental Material at http://link.aps.org/supplemental/10.1103/PhysRevLett.120.085703 for the comparison between the seeding and current methods, additional critical plateaus, and computational details, which includes Refs. [13–15].
[13] F. C. Frank, Proc. R. Soc. A **215**, 43 (1952).
[14] J. R. Espinosa, C. Vega, C. Valeriani, and E. Sanz, J. Chem. Phys. **142**, 194709 (2015).
[15] G. Chkonia, J. Wölk, R. Strey, J. Wedekind, and D. Reguera, J. Chem. Phys. **130**, 064505 (2009).
[16] J. R. Espinosa, P. Sampedro, C. Valeriani, C. Vega, and E. Sanz, Faraday Discuss. **195**, 569 (2016).
[17] M. W. Finnis and J. E. Sinclair, Philos. Mag. A **50**, 45 (1984).
[18] M. I. Mendelev, M. J. Kramer, S. G. Hao, K. M. Ho, and C. Z. Wang, Philos. Mag. **92**, 4454 (2012).
[19] M. I. Mendelev, M. J. Kramer, R. T. Ott, D. J. Sordelet, D. Yagodin, and P. Popel, Philos. Mag. **89**, 967 (2009).
[20] W. M. Brown, P. Wang, S. J. Plimpton, and A. N. Tharrington, Comput. Phys. Commun. **182**, 898 (2011).
[21] W. M. Brown, A. Kohlmeyer, S. J. Plimpton, and A. N. Tharrington, Comput. Phys. Commun. **183**, 449 (2012).
[22] W. M. Brown and M. Yamada, Comput. Phys. Commun. **184**, 2785 (2013).
[23] P. J. Steinhardt, D. R. Nelson, and M. Ronchetti, Phys. Rev. B **28**, 784 (1983).
[24] P. Rein ten Wolde, M. J. Ruiz-Montero, and D. Frenkel, J. Chem. Phys. **104**, 9932 (1996).
[25] P.-N. Tan, M. Steinbach, and V. Kumar, *Introduction to Data Mining* (Pearson Addison-Wesley, Reading, MA, 2005).
[26] J. Bokeloh, R. E. Rozas, J. Horbach, and G. Wilde, Phys. Rev. Lett. **107**, 145701 (2011).

[27] A. Filipponi, A. Di Cicco, S. De Panfilis, P. Giammatteo, and F. Iesari, Acta Mater. **124**, 261 (2017).

[28] S. R. Wilson and M. I. Mendelev, Philos. Mag. **95**, 224 (2015).

[29] M. I. Mendelev, M. J. Kramer, C. A. Becker, and M. Asta, Philos. Mag. **88**, 1723 (2008).

[30] A. Widmer-Cooper, P. Harrowell, and H. Fynewever, Phys. Rev. Lett. **93**, 135701 (2004).

[31] W. H. Wang, J. J. Lewandowski, and A. L. Greer, J. Mater. Res. **20**, 2307 (2005).

[32] Y. Li, Q. Guo, J. A. Kalb, and C. V. Thompson, Science **322**, 1816 (2008).

[33] C. Tang and P. Harrowell, Nat. Mater. **12**, 507 (2013).

Supplemental Material for "Overcoming the time limitation in molecular dynamics simulation of crystal nucleation: a persistent-embryo approach"

Yang Sun[1*], Huajing Song[1], Feng Zhang[1*], Lin Yang[1], Zhuo Ye[1],

Mikhail I. Mendelev[1], Cai-Zhuang Wang[1,2], Kai-Ming Ho[1,2,3]

[1]Ames Laboratory, US Department of Energy, Ames, Iowa 50011, USA

[2]Department of Physics, Iowa State University, Ames, Iowa 50011, USA

[3]Hefei National Laboratory for Physical Sciences at the Microscale and Department of Physics,

University of Science and Technology of China, Hefei, Anhui 230026, China

Content

[*]Electron address: yangsun@ameslab.gov (Y.S) or fzhang@ameslab.gov (F.Z.)

S1. Thresholds to determine solid-like and liquid-like atoms

Since the structural ordering generally exists in the supercooled liquid [1], it's natural that the order parameter mislabels minor atoms for solid and liquid. To choose a statistically sound threshold, we follow the strategy by Espinosa *et al.* [2] to plot the population of mislabeled atoms as a function of the threshold values in Fig. S1. The crossing point between the mislabeling curves of the liquid and solid phases is chosen as the threshold, because at this point the probability of mislabeling particles in the bulk liquid as solid-like is the same as that of mislabeling particles in the bulk solid as liquid-like.

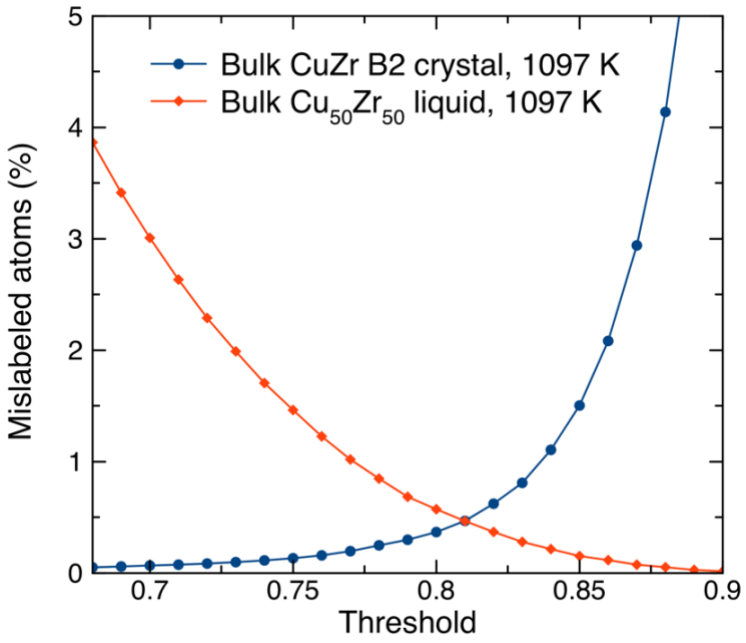

FIG. S1 Thresholds to determine solid-like and liquid-like atoms. Population of mislabeled atoms by different threshold values in bulk CuZr crystal and liquid.

S2. Critical plateaus for Ni at different temperatures

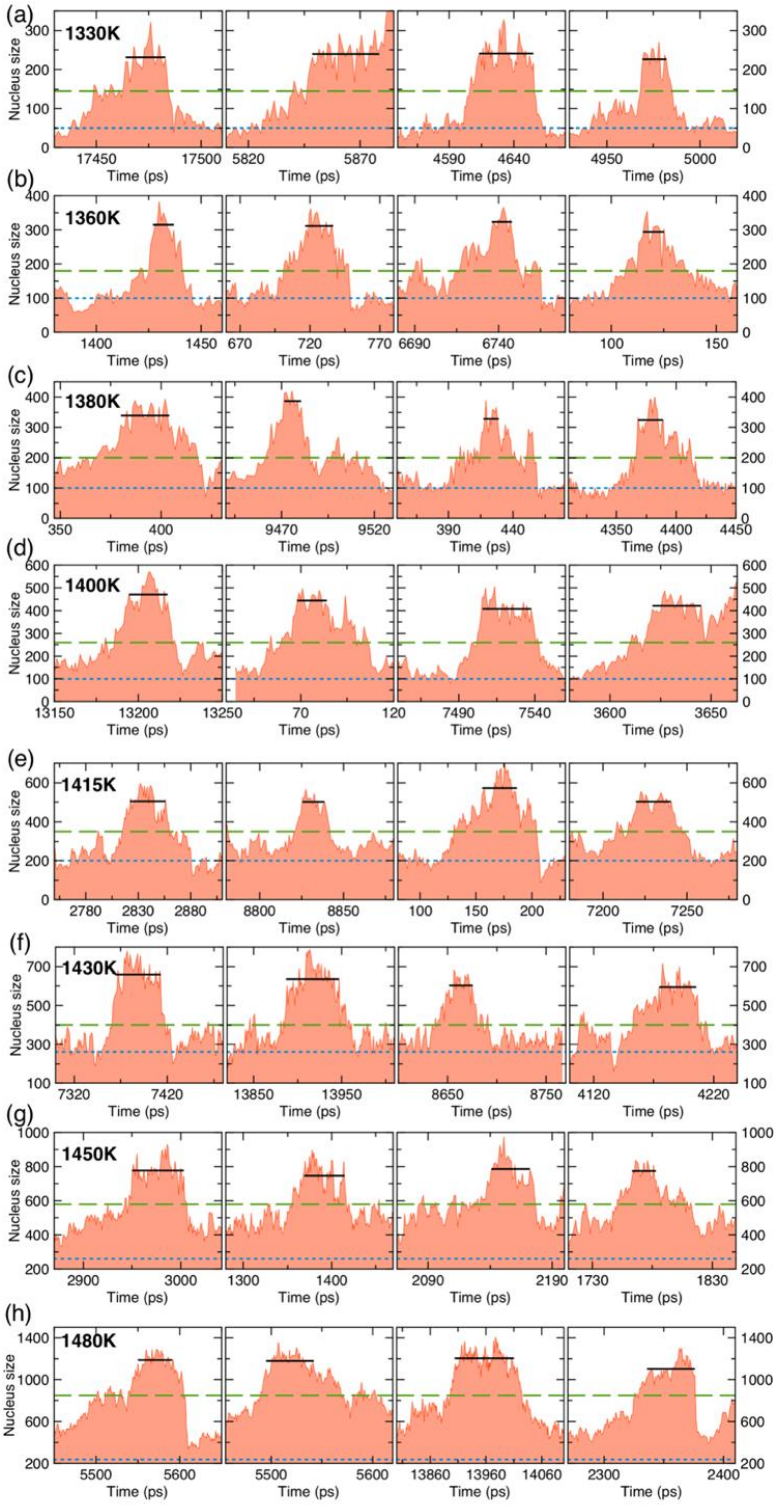

FIG. S2. The plateaus (black solid line) to determine the critical nucleus size at various temperatures for Ni. The dot line (blue) indicates the size of persistent embryo N_0 and the dash line (green) indicates the threshold N_{sc} to remove the constrain.

S3. Deriving the nucleation barrier

Conventionally, classical nucleation theory has to assume a spherical shape of nucleus, i.e. $s = \sqrt[3]{36\pi}$ in equation $\Delta G(N) = N\Delta\mu + s(N/\rho)^{2/3}\gamma$, to derive the height of barrier ΔG^* with $\Delta\mu$ and γ [3]. However, most nuclei do not form the spherical shape [4]. Note

$$\frac{\partial \Delta G(N)}{\partial N} = \Delta\mu + \frac{\partial s}{\partial N}(N/\rho)^{\frac{2}{3}}\gamma + s\gamma\rho^{-\frac{2}{3}}\frac{2}{3}N^{-\frac{1}{3}} \quad \text{(S1)},$$

and $\frac{\partial \Delta G(N^*)}{\partial N} = 0$ at the critical point. If one assumes the shape factor s is independent to the nucleus size, i.e. $\frac{\partial s}{\partial N} = 0$, the factors γ and s, which are both difficult to compute, can be canceled at the critical point as $s\gamma = -\frac{3}{2}\Delta\mu\rho^{\frac{2}{3}}N^{*\frac{1}{3}}$. Therefore,

$$\Delta G(N^*) = -\frac{1}{2}\Delta\mu N^* \quad \text{(S2)}.$$

The independent shape assumption is more real than the spherical assumption. Because the shape of the nucleus is mainly determined by the anisotropic interfacial free energy and interface mobility which is independent to the bulk size. Note for the spherical nucleus, Eqn. (S2) is also valid [2].

S4. Preparing the initial embryo

The embryo is prepared by cutting a spherical cluster from the superlattice of the equilibrated crystal (FCC-Ni and B2-$Cu_{50}Zr_{50}$ in this work). Here we examine the sensitivity of measured critical nucleus size N^* on the choice of the embryo size N_0, embryo shape and sub-critical threshold N_{sc}. The tests were performed for the model of the Ni supercooled liquid containing 32,000 atoms at 1430K. Multiple MD runs were performed to collect critical plateaus for statistical analysis. Different values of N_0 and N_{sc} are chosen to see how the critical nucleus size N^* depends on the choice of these parameters. The results are summarized in Table S1 and all the collected plateaus are shown in Fig. S3. We can see that in cases #1-5, different N_0 ($211 \leq N_0 \leq 311$) and N_{sc}

($400 \leq N_{sc} \leq 500$) parameters lead to pretty much the same critical nucleus size N^*. We also changed the shape of the embryo and found that the N^* is also not sensitive to the shape of the embryo (case #1 and #6). It should be noted that the PEM is not applicable when N_0 and N_{sc} are chosen to be too large or too small. When N_0 and N_{sc} are too large as shown in the case #7, the crystallization takes place very fast (~100 ps) so that one can hardly distinguish any clear critical plateaus that far from N_0 and N_{sc}. On the other hand, if N_0 and N_{sc} are too small as shown in the cases #8 and #9, no nucleation event or any critical plateau can be observed within the simulation time of 10 ns in all the 10 MD runs. Therefore, reasonable choice of N_0 and N_{sc} is required for the PEM to work efficiently. This can be achieved by a few trial-and-error cycles until the critical fluctuating plateau can be observed within typical MD timescale in the simulation.

Table S1 Dependence of N^* on N_0 and N_{sc}. The values in the bracket show the standard deviation.

Case	Embryo shape	N_0	Nsc	N^*
1	Sphere	261	400	623 (26)
2	Sphere	261	450	628 (16)
3	Sphere	261	500	625 (20)
4	Sphere	211	400	620 (15)
5	Sphere	311	400	626 (22)
6	Cube	261	400	627 (13)
7	Sphere	561	600	-
8	Sphere	111	400	-
9	Sphere	261	300	-

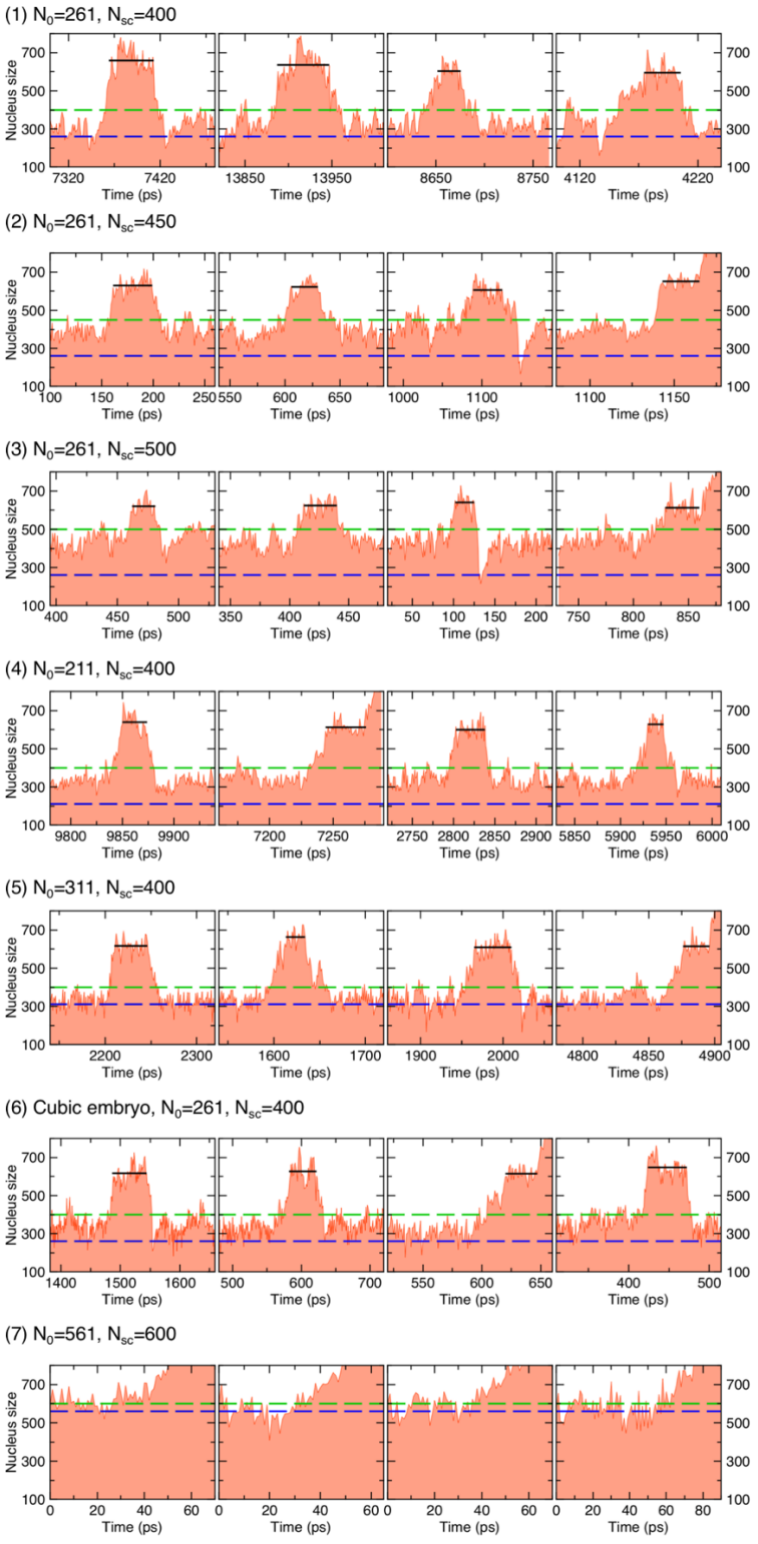

FIG. S3 The plateaus (black solid line) to determine the critical nucleus size using different N_0 and N_{sc} in persistent-embryo method for Ni at 1430 K. (1)-(7) correspond to Case #1-7 in Table S1. The blue dashed line indicates the size of the embryo N_0 and the greed dashed line indicates the threshold N_{sc} to remove the spring.

S5. The nucleation barriers of Ni and $Cu_{50}Zr_{50}$

The bulk and interfacial contributions to the nucleation barrier of the Ni and $Cu_{50}Zr_{50}$ alloy at the same reduced supercooling is provided in Table S2. The barrier ΔG^* was computed from PEM using the classical nucleation theory. According to these data, the main reason for higher nucleation barrier of the B2 phase in the $Cu_{50}Zr_{50}$ alloy is associated with much larger energy penalty of forming the liquid/B2 interface comparing to that for the liquid/fcc interface in Ni. Since nucleation rate depends exponentially on these quantities, these differences lead to 6 orders of magnitude difference on the nucleation rate.

Table S2 Quantities of nucleation barrier, as well as the contribution from bulk and interfacial terms for Ni and $Cu_{50}Zr_{50}$ at same reduced supercooling 17%. All the quantities use k_BT as the unit.

System	Nucleation barrier ΔG^* (k_BT)	Bulk term, $\Delta\mu N^*$ (k_BT)	Interfacial term, $\Delta G^* - \Delta\mu N^*$ (k_BT)
Ni at 1430 K	71.4	-142.7	214.1
$Cu_{50}Zr_{50}$ at 1097 K	85.2	-170.4	255.6

S6. Comparison between persistent-embryo method and seeding method

In order to demonstrate that the persistent-embryo method (PEM) is different from the conventional seeding method, we have performed the following simulations. First, using a spherical fcc cluster of the same size as the critical nucleation size (N^*= 623) of pure Ni at 1430 K obtained from our PEM as a seed, we performed the seeding simulation following exactly the seeding same process as described in one of the latest papers on the seeding method [5]. Then we measured the nucleation probability of the seeded cluster by repeating MD runs 10 times using the same initial configuration but different atomic velocities (isoconfigurational ensemble). As shown

in Fig. S4(a), the seeded cluster leads to solidification in only 1 out of 10 runs. In comparison, starting from a snapshot from the critical plateau containing the critical nucleus of the same size (N^*=623) obtained by the PEM, the same MD runs gave 5/10 probability for solidification. Next, we varied the size of seeded clusters in the seeding simulations to find the right seed size that can give 50% probability of crystallization (the criteria for determining critical nucleus size). The procedure was repeated for several temperatures. Figure S4(b) shows that the seeding method systematically overestimates the critical nucleus size comparing to the results using PEM. The overestimation of the critical nucleus size by the seeding method leads to a systematic underestimation of the nucleation rate by 2-4 orders of magnitude comparing to the results from the PEM as shown in Fig. S4(c). These results clearly demonstrate that the PEM presented in our paper is very different from the conventional seeding method.

To further demonstrate the accuracy of PEM as compared with the seeding method, we fit the nucleation rate data collected in the moderately supercooled regime to the empirical function proposed in Ref. [6]:

$$J(T) = \Gamma \exp\left[-\frac{BT^2}{(T_m - T)^2}\right]. \quad \text{(S3)}$$

where Γ and B are fitting parameters and T_m is the melting temperature. Based on the fitting, the nucleation rates are then extrapolated to deeply supercooled region and compared with the nucleation rate data obtained by brute-force MD simulations using the mean first-passage time (MFPT) method [7]. The nucleation rates of the same system at different temperature ranges are expected to form a smooth curve. Figure R4(c) shows that the extrapolation from the PEM data leads to an excellent agreement with the brute-force MD data, while the extrapolation from the seeding method data leads to systematic underestimation of the nucleation rate by ~3 orders of

magnitudes. These results indicate that our PEM is more accurate than the conventional seeding method in determination of nucleation rates.

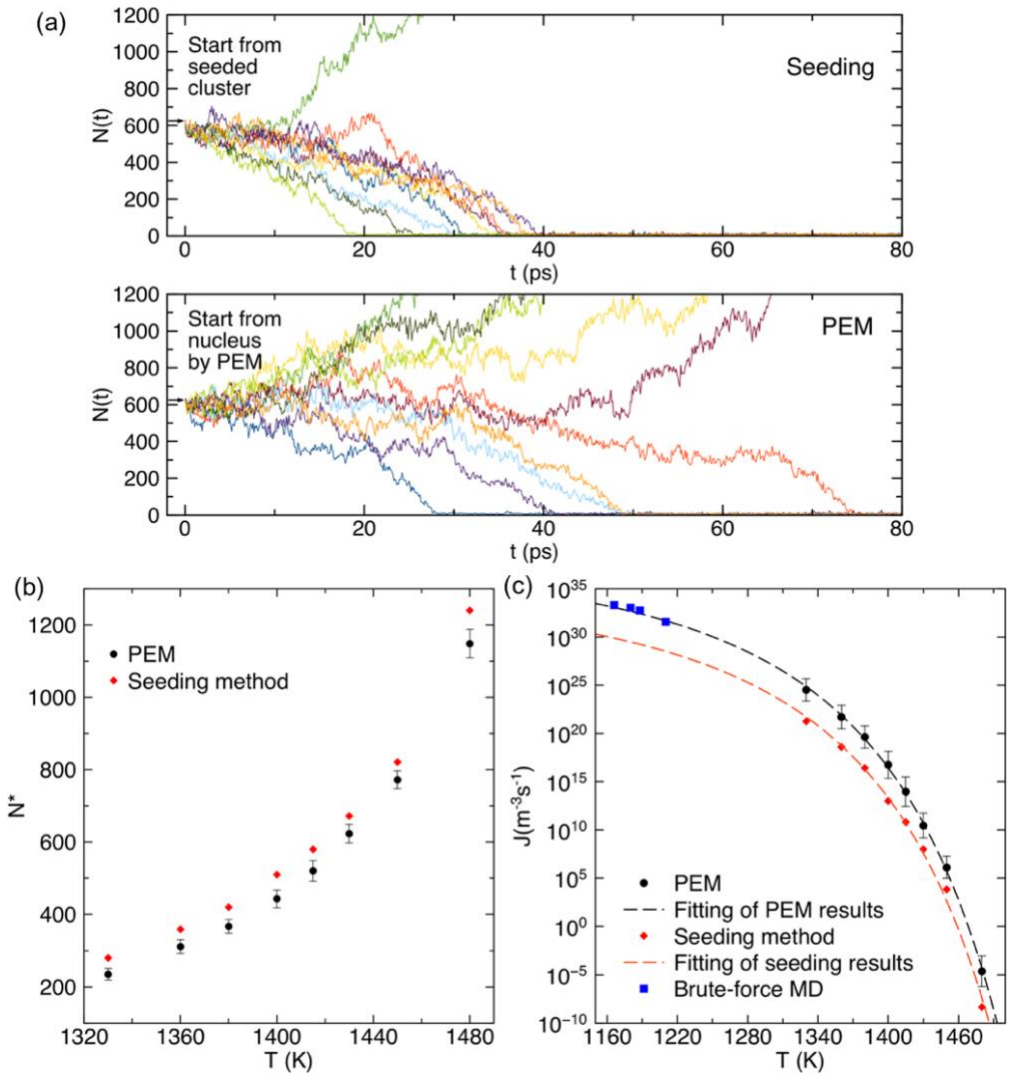

FIG. S4 (a) nucleus size versus time for 10 trajectories by seeding method (upper panel) and PEM (lower panel). Each color indicates one MD trajectory. (b) Comparison of critical nucleus size obtained by seeding method and PEM. (c) Comparison of nucleation rate obtained by seeding method (red) and PEM (black). The blue square shows the nucleation rate obtained by brute-force MD with MFPT method at deeply supercooled region. The dashed lines show the fitting and extrapolation of the seeding and PEM data to deep supercooling using Eqn. (S3).

Supplementary References

[1] F. C. Frank, Proc. R. Soc. A **215**, 43 (1952).

[2] J. R. Espinosa, C. Vega, C. Valeriani, and E. Sanz, J. Chem. Phys. **144**, 034501 (2016).

[3] K. F. Kelton and A. L. Greer, *Nucleation in Condensed Matter: Application in Materials and Biology* (Elsevier, Amsterdam, 2010).

[4] G. C. Sosso, J. Chen, S. J. Cox, M. Fitzner, P. Pedevilla, A. Zen, and A. Michaelides, Chem. Rev. **116**, 7078 (2016).

[5] J. R. Espinosa, C. Vega, C. Valeriani, and E. Sanz, J. Chem. Phys. **142**, 194709 (2015).

[6] J. Bokeloh, R. E. Rozas, J. Horbach, and G. Wilde, Phys. Rev. Lett. **107**, 145701 (2011).

[7] G. Chkonia, J. Wölk, R. Strey, J. Wedekind, and D. Reguera, J. Chem. Phys. **130**, 64505 (2009).